Acta Crystallographica Section D
Biological Crystallography
ISSN 0907-4449

Structure of SRP14 from the *Schizosaccharomyces pombe* signal recognition particle

Mark A. Brooks,[a] Raimond B. G. Ravelli,[b] Andrew A. McCarthy,[c] Katharina Strub[d] and Stephen Cusack[c]*

[a]IBBMC–CNRS UMR8619, Bâtiment 430, Université de Paris-Sud, 91405 Orsay, France, [b]MCB–EM, Leiden University Medical Center, PO Box 9600, 2300 RC, Leiden, The Netherlands, [c]European Molecular Biology Laboratory – Grenoble Outstation, BP 181, Grenoble CEDEX 9, France, and [d]Département de Biologie Cellulaire, Université de Genève, Sciences III, 1211 Geneva, Switzerland

Correspondence e-mail: cusack@embl.fr

Received 29 September 2008
Accepted 16 February 2009

PDB Reference: SRP14, 2w9j, r2w9jsf.

The signal recognition particle (SRP) *Alu* domain has been implicated in translation elongation arrest in yeasts and mammals. Fission yeast SRP RNA is similar to that of mammals, but has a minimal *Alu*-domain RNA lacking two stem-loops. The mammalian *Alu*-domain proteins SRP9 and SRP14 bind their cognate *Alu* RNA as a heterodimer. However, in yeasts, notably *Saccaromyces cerevisiae*, SRP14 is thought to bind *Alu* RNA as a homodimer, the SRP9 protein being replaced by SRP21, the function of which is not yet clear. Structural characterization of the *Schizosaccharomyces pombe Alu* domain may thus help to identify the critical features required for elongation arrest. Here, the crystal structure of the SRP14 subunit of *S. pombe* SRP (SpSRP14) which crystallizes as a homodimer, is presented. Comparison of the SpSRP14 homodimer with the known structure of human SRP9/14 in complex with *Alu* RNA suggests that many of the protein–RNA contacts centred on the conserved U-turn motif are likely to be conserved in fission yeast. Initial attempts to solve the structure using traditional selenomethionine SAD labelling failed. However, two As atoms originating from the cacodylate buffer were found to make cysteine adducts and strongly contributed to the anomalous substructure. These adducts were highly radiation-sensitive and this property was exploited using the RIP (radiation-damage-induced phasing) method. The combination of SAD and RIP phases yielded an interpretable electron-density map. This example will be of general interest to crystallographers attempting *de novo* phasing from crystals grown in cacodylate buffer.

1. Introduction

The signal recognition particle (SRP) is a ribonucleoprotein particle found in all kingdoms of life which is responsible for the targeting of nascent polypeptides to either the prokaryotic plasma membrane or the eukaryotic endoplasmic reticulum (ER; Blobel & Dobberstein, 1975*a*,*b*). Newly translated peptides are thus directed to their target membrane for either membrane insertion or secretion, collectively termed 'protein translocation'. SRPs are composed of between one (in some prokarya) and six (in most eukarya) polypeptides bound to a central RNA molecule (Keenan *et al.*, 2001).

The mechanism of action of SRP was first described in the mammalian system. Ribosome-associated SRP detects and binds to nascent polypeptides, which bear hydrophobic signal sequences, as they emerge from the ribosomal exit site as the initial step of the SRP cycle. In eukaryotes, this interaction induces a transient delay in further translation, which provides a time window for the ribosome–nascent chain complex (RNC) to be targeted to the ER membrane (Walter & Blobel, 1981;

© 2009 International Union of Crystallography
Printed in Singapore – all rights reserved

Lakkaraju *et al.*, 2008). There, the RNC binds to the heterodimeric SRP receptor (SR) in complex with the translocation channel (translocon; Gilmore *et al.*, 1982). In a GTP-regulated process, the SR triggers the release of SRP from the ribosome and the signal peptide, with concomitant transfer of the signal peptide to the translocon. Translation then resumes and drives translocation (Connolly *et al.*, 1991).

The eukaryotic SRP is composed of two domains: the *Alu* domain and the S domain. The universally conserved S domain is responsible for the recognition of signal peptides as well as for the interaction with the SR, whereas the *Alu* domain has been shown in eukaryotes to be responsible for a delay in nascent chain elongation. The delay is essential for efficient translocation because it maintains the nascent peptide in a state competent for interaction with the translocation channel and prevents premature folding (Lakkaraju *et al.*, 2008). The human *Alu* domain is composed of a heterodimer of SRP9 and SRP14 proteins bound to *Alu* RNA, which comprises the 3′ and 5′ ends of SRP RNA. The central part of SRP RNA constitutes the S-domain RNA, onto which the remaining SRP subunits (SRP68/72 and SRP19/54 in mammals and yeast) are assembled.

A basic motif of five amino-acid residues within the C-terminal tail of SRP14 is critical for the elongation-arrest function, but the mechanism by which this occurs remains to be established (Thomas *et al.*, 1997; Lakkaraju *et al.*, 2008; Mason *et al.*, 2000). The cryo-EM structure of an artificially arrested SRP–ribosome–nascent chain complex, cross-linking studies during the course of translation and genetic studies suggested that the SRP *Alu* domain may interfere with the functions of the elongation factor eEF2 (Ogg & Walter, 1995; Terzi *et al.*, 2004; Halic *et al.*, 2004).

The X-ray structure of the murine SRP9/14 dimer demonstrated that both proteins possessed a novel fold with an $\alpha\beta\beta\beta\alpha$ topology termed the *Alu*-binding motif (Birse *et al.*, 1997). These subunits associate to form a pseudo-symmetric heterodimer which forms a complex with its cognate RNA by specifically recognizing a conserved U-turn sequence (Strub & Walter, 1990). Additionally, the human SRP9/14 heterodimer has been solved in complex with two synthetic *Alu* RNAs, which revealed that the complex may exist in two states: a high-affinity conformation and a low-affinity conformation (Weichenrieder *et al.*, 2000, 2001).

The subunit compositions of the fission and budding yeast SRPs resemble that of human SRP (Brown *et al.*, 1994; Selinger *et al.*, 1994), except that these fungal SRPs lack homologues of SRP9 and contain an additional subunit: SRP21. In addition, SRP14 has been shown to bind to the RNA as a homodimer *in vitro* and *in vivo* (Strub *et al.*, 1999; Mason *et al.*, 2000) and the footprint of this homodimer is similar to that of human SRP9/14 on its cognate RNA, including the conserved UGU U-turn motif (Strub *et al.*, 1999). When compared with human SRP RNAs, some fungal sequences are longer (*e.g.* scR1 SRP RNA of *Saccharomyces cerevisiae*), whereas others are slightly shorter (*e.g.* s1r1 SRP RNA of *Schizosaccharomyces pombe*). In both of these cases the *Alu* domain is simpler in that it lacks helices 3 and 4 (Fig. 1) of the human *Alu* domain. SRP21 has weak but significant sequence similarity to SRP9, suggesting a common origin for these proteins (Rosenblad *et al.*, 2004). The authors also suggested that the metazoan SRP9 and fungal SRP21 subunits were not merely structurally related but were also functionally orthologous, implying that an SRP21/SRP14 heterodimer exists in yeast.

We decided to test whether SRP14 from *S. pombe* (henceforth referred to as SpSRP14) could interact with *S. pombe* SRP21 (SpSRP21) by performing crystallization screening of various truncation mutants of SpSRP14 alone as well as when copurified with truncation mutants of SpSRP21. Interestingly, SpSRP21 had a tendency to degrade, leaving SpSRP14 to crystallize alone. Such crystals diffracted to 2.6 Å resolution and allowed us to solve the structure of SpSRP14, showing that it forms a homodimer. High structural conservation is centred on the residues in the β-sheet of SpSRP14 that make contacts with the U-turn sequence of the RNA in the structure of human SRP9/14 in complex with *Alu* RNA. This indicates that RNA recognition by a homodimer of SpSRP14 is likely to be generally similar to that in the human system.

An increasing number of strategies have been developed to exploit intrinsic sources of anomalous scattering in order to solve macromolecular structures; for example, utilizing the anomalous dispersion of sulfur-containing residues or bound heavy atoms. In this case, arsenic in the form of dimethylarsenate had reacted serendipitously with the free sulfhydryl groups of SpSRP14 during crystallization to form a cacodylate–cysteine adduct. Each molecule of SpSRP14 contains one initiating methionine and two cysteine residues which would be expected to be available for heavy-atom substructure determination, if all indeed contained heavy atoms. Therefore, we used a data-collection strategy at the Se *K* absorption edge, where there is also significant anomalous scattering from arsenic, thus allowing the identification of the selenium- and arsenic-containing heavy-atom substructure. In this way, poor initial phases were obtained using data collected from crystals which contained selenium-labelled protein by single-wavelength anomalous dispersion (SAD). However, when additional phase information from radiation-damaged-induced phasing (RIP) was included (Ramagopal *et al.*, 2005; Ravelli *et al.*, 2003; Nanao *et al.*, 2005; Banumathi *et al.*, 2004; Zwart *et al.*, 2004; Evans *et al.*, 2003), the resulting electron-density maps were dramatically improved. Whereas the electron density calculated from SAD phases was interpretable only in parts, the maps produced using combined SAD and RIP phases permitted automatic building programs to trace almost the entire C^{α} backbone of the model. The applicability of this type of phasing strategy to other structures is discussed.

2. Experimental procedures

2.1. Cloning of the *S. pombe* genes encoding SRP21 and SRP14 for expression singly

In order to clone the gene of SpSRP14, PCR was performed using a template of *S. pombe* genomic DNA purified essen-

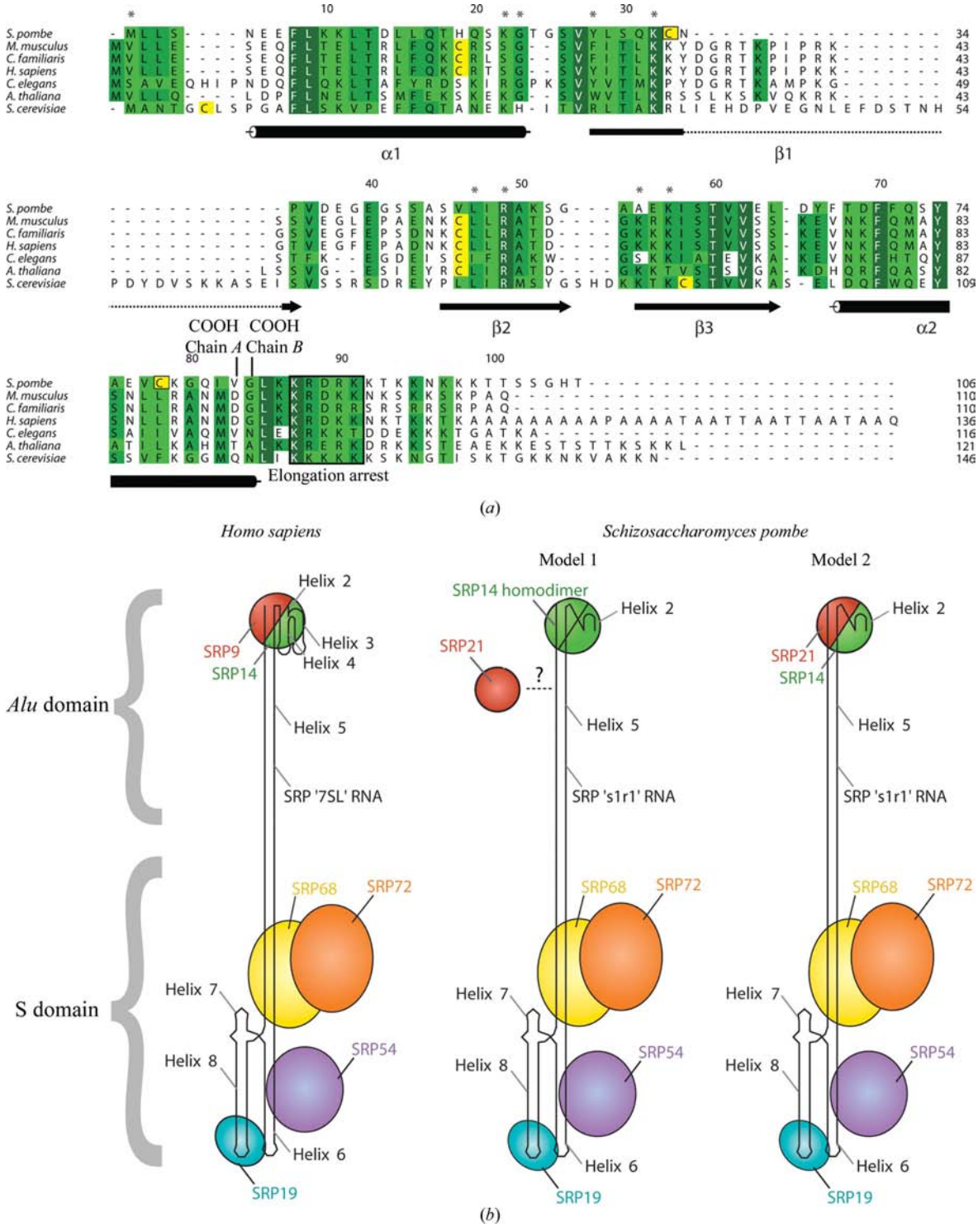

Figure 1
(*a*) Sequence alignment of the SRP14 proteins of *Arabidopsis thaliana*, *Caenorhabditis elegans*, *Canis familiaris*, *Homo sapiens*, *Mus musculus*, *Saccharomyces cerevisiae* and *Schizosaccharomyces pombe*. SRP14 sequences were aligned with *ClustalX* (Thompson *et al.*, 1997) and formatted with *ALSCRIPT* (Barton, 1993). Aligned residues are highlighted according to the conservation scores of Zvelebil *et al.* (1987) according to these criteria: positions with a score of >4, light green; score of >5, mid-green; strictly conserved residues, dark green with white lettering. Sequences are numbered according to *S. pombe* SRP14. Cysteine residues are shown in yellow and such residues of *S. pombe* Srp14 are boxed. Also boxed is the sequence which has been shown to be essential for elongation arrest (Thomas *et al.*, 1997; Mason *et al.*, 2000; Lakkaraju *et al.*, 2008), which is labelled 'Elongation arrest'. The structure presented here is disordered in this region; the carboxy-terminal residues which are ordered are labelled 'COOH' for chain *A* and chain *B*. Amino acids which are likely to interact with *Alu*-domain RNA are highlighted with grey asterisks. (*b*) Schematic diagrams of SRPs from human and *S. pombe*. The *Alu* and S domains are labelled. Of particular note are the differences between the two particles in terms of the subunit compositions of the *Alu* domains. While human SRPs have a pseudo-symmetrical SRP9/14 complex, *S. pombe*, like other fungi, is believed to possess a homodimer of SRP14 subunits, as shown in Model 1. Model 2 depicts the possible subunit composition of SRP proposed by Rosenblad *et al.* (2004), in which SRP14 heterodimerizes with SRP21. See text for further discussion.

tially as described previously for *Saccharomyces cerevisiae* (Rigaut *et al.*, 1999). After cloning into an expression vector, an intron was removed by inverse PCR (Maniatis *et al.*, 1982) and the product of this reaction was phosphorylated with T4 polynucleotide kinase (Roche Diagnotics, Basel, Switzerland) and circularized with T4 ligase, generating the plasmid pETM11::SpSRP14[1–106].

To clone SpSRP21, RT-PCR was performed using *S. pombe* total RNA as template (Moreno *et al.*, 1991). First-strand cDNA was produced using AMV reverse transcriptase according to the manufacturer's instructions (Promega Corp., Madison, Wisconsin, USA) and was then used as a template to amplify the gene encoding the first 119 amino-acid residues of SpSRP21 (the remaining residues of SRP21 were avoided since they consist of a polylysine region, which was considered to have a high propensity for disorder). Finally, the product of the above PCR reaction was cloned into the *Nco*I and *Kpn*I sites of pET-M11, yielding the vector pETM11::SpSRP21[1–112]. However, the resulting protein was insoluble

Table 1
Crystallographic and data-collection statistics.

Values in parentheses are for the highest resolution shell.

Data set	1	2	3	Native
Beamline	ID23-1	ID23-1	ID23-1	ID14-4
Wavelength (Å)	0.978	0.978	0.978	0.939
Space group	$P3_221$	$P3_221$	$P3_221$	$P3_221$
Unit-cell parameters (Å)	$a = b = 57.69$, $c = 86.09$	$a = b = 57.74$, $c = 86.11$	$a = b = 57.74$, $c = 86.06$	$a = b = 57.06$, $c = 86.39$
Resolution limits (Å)	50.0–2.6 (2.7–2.6)	50.0–2.6 (2.7–2.6)	50.0–2.6 (2.7–2.6)	50.0–2.6 (2.7–2.6)
Reflections measured	27048 (2035)	27201 (2022)	27209 (2040)	30227 (3239)
Unique reflections measured	5285 (473)	5289 (472)	5283 (473)	5174 (525)
Completeness (%)	97.5 (83.6)	97.6 (84.0)	97.3 (82.7)	97.4 (95.5)
$\langle I\rangle/\langle\sigma(I)\rangle$	15.7 (6.6)	17.0 (6.3)	14.9 (5.4)	16.42 (5.0)
$R_{\rm merge}$† (%)	6.1 (19)	5.4 (20.9)	6.1 (24.3)	6.2 (41.4)

† $R_{\rm merge} = \sum_{hkl}\sum_i |I_i(hkl) - \langle I(hkl)\rangle|/\sum_{hkl}\sum_i I_i(hkl)$, where $\langle I(hkl)\rangle$ is the mean intensity of reflection $I(hkl)$ and $I_i(hkl)$ is the intensity of an individual measurement of reflection $I(hkl)$.

2.2. Co-expression and copurification of *S. pombe* SRP21 and SRP14 using pST39

A vector permitting translation of up to four proteins from a single polycistron in an approximately stoichiometrically equivalent manner was chosen for co-expression (Tan, 2001). The co-expression plasmid was transformed into *Escherichia coli* BL21(DE3) cells, but the cultures grew slowly and did not appear to express the recombinant proteins (not shown). In order to repress the basal level of recombinant protein production, another *E. coli* strain, BL21-AI, was tested. In this case, a tighter control of the expression of T7 RNA polymerase production by the araBAD promoter has been reported (Boomershine *et al.*, 2003). Under these conditions, cell cultures expressed both SpSRP21 and SpSRP14 to a high level and yielded approximately 5 g wet cell paste per litre of medium.

2.3. Purification of the *S. pombe* SRP21/SRP14 complex

Since the purified SRP21 and SRP14 were to be used in crystallization trials, purification tags which could contribute disordered regions were avoided. Instead, the purification strategy was based upon those of the mouse and human proteins (Birse *et al.*, 1997; Weichenrieder *et al.*, 2000). Cell paste corresponding to 1 l culture was sonicated in solution containing 10 m*M* HEPES pH 7.5, 5 m*M* $MgCl_2$, 400 m*M* NaCl, 5 m*M* dithioethreitol) supplemented with Complete protease inhibitors (Roche Diagnotics, Basel, Switzerland). Following centrifugation (13 000*g*, 30 min), the supernatant was filtered through 3MM paper (Whatman), loaded onto a HiPrep Heparin Sepharose 16/10 column (GE Healthcare) and eluted with buffer containing 1 *M* NaCl. Peak fractions were then diluted approximately tenfold in buffer composed of 10 m*M* HEPES pH 7.5, 5 m*M* $MgCl_2$, 200 m*M* NaCl, 5 m*M* dithioethreitol and applied onto an SP Sepharose column (GE Healthcare) which had been equilibrated with this buffer. Protein was eluted with a salt gradient up to 1 *M* NaCl. Peak fractions were pooled and purified using a Superdex 75 16/60 prep-grade column (GE Healthcare) in solution containing 10 m*M* HEPES pH 7.5, 5 m*M* $MgCl_2$, 200 m*M* NaCl and 5 m*M* dithioethreitol and peak fractions were pooled. Separation of the resulting fractions by SDS–PAGE followed by visualization using Coomassie indicated that SpSRP21 and SpSRP14 copurified at all stages in apparently stoichiometrically equivalent amounts (data not shown).

2.4. Crystallization

Screening for conditions under which each of the SRP21 and SRP14 deletion constructs would crystallize was performed by the vapour-diffusion method using proprietary screens (Hampton Research). Proteins were purified and concentrated to between 5 and 15 mg ml^{-1} in Ultrafree 5 kDa molecular-weight cutoff microconcentrators (Millipore). 1 µl of such protein samples was then mixed with an equal volume of reservoir solution and allowed to equilibrate.

Crystallization using protein co-expressed and copurified from the construct pST39::SRP21[1–81]:SRP14[1–91] was performed using the hanging-drop vapour-diffusion method at 294 K. SRP21 tended to degrade during purification, leaving SRP14 to crystallize alone. A sparse-matrix screen allowed initial crystallization conditions to be obtained (Natrix Screen condition No. 25, Hampton Research; 50 m*M* sodium cacodylate pH 6.5, 30% PEG 4000 and 80 m*M* magnesium acetate). Crystals appeared within 1 d and were of hexagonal cross-section. Grid screening was used to improve the crystals and the composition of the reservoir solution in the refined crystallization conditions was 50 m*M* cacodylic acid pH 6.5, 22% PEG 4000 and 50 m*M* sodium acetate.

2.5. Data collection

Soaking the crystals in a cryoprotectant (50 m*M* MES pH 6.5, 20% PEG 4000, 50 m*M* sodium acetate and 30% glycerol) allowed them to be flash-frozen at 100 K prior to exposure to X-rays. Data were collected on ESRF beamline ID14-4 for the native data set at a wavelength of 0.939 Å and on beamline ID23-1 at a wavelength of 0.978 Å for data sets obtained using selenium-labelled crystals, with a 1° oscillation per frame. Data were recorded using charge-coupled device detectors: ADSC Q4R at ID14-4 and a 225 mm detector (MAR Research) at ID23-1. Three data sets of 90° were recorded with starting angles determined using the *XPLAN* routine of *XDS* (Kabsch, 1993). This data-collection strategy has proved useful locally in cases where the anomalous signal has been degraded by radiation damage (Ravelli *et al.*, 2005). It has been shown that SAD phases may then be improved by the incorporation of RIP phases with a view to producing unimodal joint phase probability distributions. However, we did not know *a priori* whether or not radiation damage was occurring. Data processing was performed using *XDS* and *XSCALE*, as well as using the *CCP*4 suite of programs (Collaborative Computational Project, Number 4, 1994). The crystals belonged to the trigonal space group $P3_221$ and statistics of the data collection are summarized in Table 1.

2.6. Structure solution and model refinement

Attempts at molecular replacement using search models based on human and murine SRP14 were unsuccessful using various programs. Instead, preliminary phases were obtained using single-wavelength anomalous dispersion (SAD). The locations of the heavy-atom sites were determined using *SHELXD* (Sheldrick, 2008) and these sites were refined using *SHARP* (de La Fortelle & Bricogne, 1997). All heavy atoms were treated as selenium throughout the phasing process. Additional phase information was obtained using RIP and phasing statistics are summarized in Table 2.

Refinement of the SpSRP14 structure was performed using *REFMAC*, with one TLS group per chain (Murshudov *et al.*, 1997), from the *CCP*4 suite of programs (Collaborative Computational Project, Number 4, 1994), with intermittent rounds of model building with *Coot* (Emsley & Cowtan, 2004) and *O* (Jones *et al.*, 1991). Validation of the structure was performed using *MOLPROBITY* (Davis *et al.*, 2004). Statistics of the refinement are summarized in Table 3.

3. Results

3.1. Crystallization and structure solution of *S. pombe* SRP14

Fission yeast SRP14 was co-expressed and copurified with SpSRP21, but the latter protein had a tendency to degrade over time. To ascertain the identity of the protein(s) which had crystallized, crystals were subjected to SDS–PAGE and mass spectrometry. In these analyses only SRP14 was positively identified, which indicated that it had crystallized alone. The crystallization of SpSRP14 was reproducible in only one condition and the resulting crystals varied extensively in their X-ray diffraction high-resolution limits (3–10 Å). Selenomethionine-labelled crystals were also produced which were of a similar morphology to those grown from native protein.

Table 2
Phasing statistics from the SAD and RIP components of the experiment.

Source of phase information	SAD	RIP
Resolution range (Å)	32.6–3.0	32.6–3.0
No. of sites	6	4
Phasing power† (acentric, anomalous)	1.93	—
Phasing power† (isomorphous, acentric/centric)	—/—	0.995/0.782
Figure of merit‡ (acentric/centric)	0.409/—	0.264/0.379

† Phasing power = $(\sum_{hkl} |F_{\rm H,calc}|^2 / \sum_{hkl} |E|^2)^{1/2}$, where $F_{\rm H,calc}$ is the calculated heavy-atom scattering factor and E is the lack-of-closure error. ‡ Figure of merit = $[\int_{\alpha=0}^{2\pi} P(\alpha)\exp(i\alpha)\,{\rm d}\alpha]/[\int_{\alpha=0}^{2\pi} P(\alpha)\,{\rm d}\alpha]$, where α is the phase and $P(\alpha)$ is the phase probability distribution.

Table 3
Refinement statistics.

Asymmetric unit content	2 protomers, 143 residues, 4 waters
Resolution range for refinement (Å)	32.6–2.6
$R_{\rm cryst}/R_{\rm free}$† (%)	0.238/0.281
R.m.s.d. bonds (Å)	0.01
R.m.s.d. angles (°)	1.243
$\langle B\rangle$ (all atoms/waters) (Å^2)	61.6/50.3
Ramachandran plot (%)	
Favoured	96.4
Allowed	3.60

† $R_{\rm cryst} = \sum_{hkl} |F_{\rm o} - F_{\rm calc}| / \sum_{hkl} |F_{\rm o}|$, where $F_{\rm o}$ is the observed structure-factor amplitude and $F_{\rm calc}$ is the calculated structure-factor amplitude. $R_{\rm free}$ is as $R_{\rm cryst}$ but for 5% of structure-factor amplitudes which were set aside during refinement.

Three successive low-redundancy but relatively complete data sets were collected at the Se *K* edge in a single-wavelength anomalous dispersion (SAD) experiment (90 frames, 1° oscillation per frame). The data-collection statistics from the three SAD data sets and a single native data set are summarized in Table 1 and show that the data for the phasing experiment are not perfectly complete, notably in the highest resolution shell, but were nonetheless sufficient for the location of heavy-atom sites. This type of data-collection strategy contrasts with that of a typical SAD experiment in which a single high-redundancy data set is collected, but also allows the experimenter to produce a higher redundancy data set by merging all three data sets together (Ravelli *et al.*, 2005). After data reduction, *SHELXD* located six heavy atoms based on the anomalous differences calculated from a combined data set composed of all three data sets in a SAD experiment (Sheldrick, 2008). The coordinates, occupancies and *B* factors of the heavy atoms were then refined against the anomalous differences and initial phases were calculated using *SHARP* (La Fortelle & Bricogne, 1997).

In order to derive additional phase information, radiation-damage-induced phasing (RIP) was employed (Ravelli *et al.*, 2003). This phasing strategy permits the identification of sites of pronounced specific radiation damage in an experiment similar to multiple isomorphous replacement (MIR; Kendrew *et al.*, 1958). Instead of a heavy-atom derivative, the first data set is taken to be a pseudo-heavy-atom 'derivative' since it is assumed to be the most electron-rich. The third of the data sets was used as a pseudo-native data set.

Calculation of a radiation-damage-induced isomorphous difference Fourier map using the initial SAD phases allowed the identification of specific radation-damage-susceptible sites. *SHARP* was used to refine the positions of these sites, effectively in a single isomorphous replacement (SIR) protocol. Phases obtained from this substructure, again calculated using *SHARP*, were combined with the SAD phases using *SIGMAA* (Read, 1986). Histogram matching and solvent flattening as implemented in the program *DM* (Cowtan, 1994) yielded a high-quality electron-density map which was easily traceable. A partial model was built into this density using the program *RESOLVE* (Terwilliger, 2003*a*) and consisted of most of the main chain as polyalanine residues with some aromatic residues docked into the sequence.

The remainder of the residues and side chains which had not been built automatically were then constructed manually. The model has an $R_{\rm cryst}$ of 0.238 and an $R_{\rm free}$ of 0.281 using reflections in the resolution range 32.6–2.6 Å. The relatively high $R_{\rm free}$ value is at least partly a consequence of the fact that a significant fraction of the protein is disordered. Despite this being a space group which permits merohedral twinning, tests using various analysis programs, for example *TRUNCATE* (Collaborative Computational Project, Number 4, 1994), did not detect significant twinning. Statistics of data collection and reduction, refinement and validation of the final molecular model of SpSRP14 with *MOLPROBITY* (Davis *et al.*, 2004) are shown in Table 3.

3.2. Overall structure of *S. pombe* SRP14

S. pombe SRP14 has an *Alu*-binding motif fold, which has been described previously (Birse *et al.*, 1997; Weichenrieder *et al.*, 2001) and has an $\alpha1$-$\beta1$-$\beta2$-$\beta3$-$\alpha2$ topology (Fig. 2*a*). There are two molecules in the asymmetric unit and relation of the two chains by a crystallographic twofold symmetry operator generates a dimer which possesses a saddle-shaped six-stranded β-sheet with proper twofold molecular symmetry (Fig. 2*b*). In contrast to the SRP9/14 structure, in which four β-strands are contributed by each of the heterologous (but orthologous) subunits, here three strands are contributed by each identical polypeptide. The β-strand βN, which has only been observed in structures of SRP14 to date (Birse *et al.*,

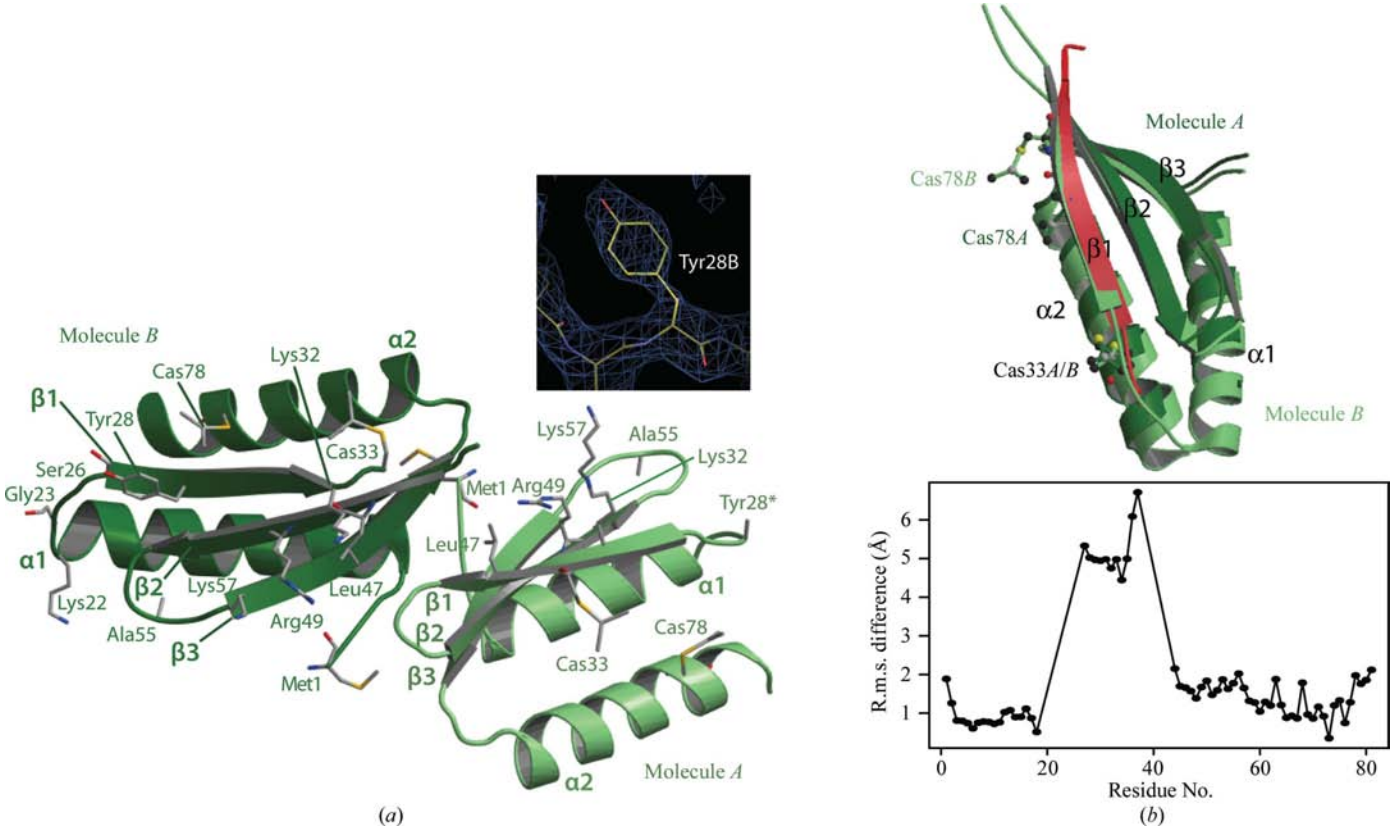

Figure 2
(*a*) Structure of the two noncrystallographically related monomers in the asymmetric unit: molecule *A* is shown at the lower right of the figure in light green and molecule *B* is shown in dark green at the upper left. Cartoon representations are in green, whereas structurally important residues are shown as sticks. The colouring of the sticks is as follows: blue, nitrogen; yellow, sulfur; carbon, grey. See text for further details. The inset depicts representative electron density around Tyr28 of chain *B* contoured at 1σ. (*b*) Chain *A* and chain *B* of *S. pombe* were superposed using *LSQKAB* (Collaborative Computational Project, Number 4, 1994). Chain *A* is coloured according to the root-mean-square displacements (r.m.s.d.s) of the C^{α} atoms (from 6.7 Å, red, to 0 Å, dark green) relative to molecule *B* (light green). Below, the r.m.s.d. values are plotted as a function of residue number. It can be seen that there is a significant displacement of the first β-strand (residues 27–37). This figure, as well as Figs. 3(*a*), 4 and 6, was produced using *MOLSCRIPT* and *BOBSCRIPT* (Kraulis, 1991; Esnouf, 1997).

1997; Weichenrieder *et al.*, 2000), appears to be skewed away from the plane of the sheet in this structure and does not participate in the hydrogen-bonding pattern of a canonical β-sheet (Fig. 2).

Chain *A* is more disordered than chain *B*, with fewer visible residues in the electron-density map; clear density is only visible for residues 1–19, 27–38 and 44–83 of chain *A* compared with residues 1–37 and 40–84 of chain *B*. Also, more side chains of chain *A* are disordered than of chain *B* (residues 19, 28, 38 and 63 of chain *A* and residue 40 of chain *B* were modelled by truncating them at the C^{β} atoms) and chain *A* has a higher mean temperature factor (67.3 and 56.5 Å^2 for chains *A* and *B*, respectively). In common with the murine and human SRP14 structures, the internal loop between β1 and β2 was partially disordered (Fig. 3) and has been predicted to become structured only upon binding to cognate RNA (Birse *et al.*, 1997; Weichenrieder *et al.*, 2000).

Short basic sequences in the carboxy-termini of mouse and yeast SRP14 have been shown to be necessary for elongation-arrest activity (Fig. 1*a*; Thomas *et al.*, 1997; Mason *et al.*, 2000; Lakkaraju *et al.*, 2008). In *S. pombe*, this sequence corresponds to residues 87–91 and, despite the fact that the SpSRP14 expression construct included these residues, it is once again unstructured as had been found in the two preceding SRP14 structures. Collectively, these results indicate that the elongation-arrest sequence is intrinsically disordered. This may be important for its functional role; its freedom of movement may be beneficial when searching for its binding site and only upon binding would this sequence become ordered.

3.3. Cacodylate-mediated crystal contacts and flexibility of sheet β1

Visual inspection of the initial electron-density maps showed prominent and continuous density for the cysteine side chains, indicating the presence of covalent modifications of the sulfhydryl groups. These features were also among the highest peaks in anomalous difference maps, indicating that they were heavy atoms (data not shown). Cacodylic acid (dimethylarsenate, hereafter referred to as Cas) may be reduced by thiols to form a reactive intermediate which fixates onto cysteine residues by mercaptan exchange (Maignan *et al.*, 1998; Greenwald *et al.*, 1999). From this evidence, it appeared likely that dimethylarsenate from the cacodylate buffer used to crystallize SpSRP14 had formed covalent bonds with the S^{γ} of each cysteine residue, thus providing heavy atoms which were then useful during experimental phasing.

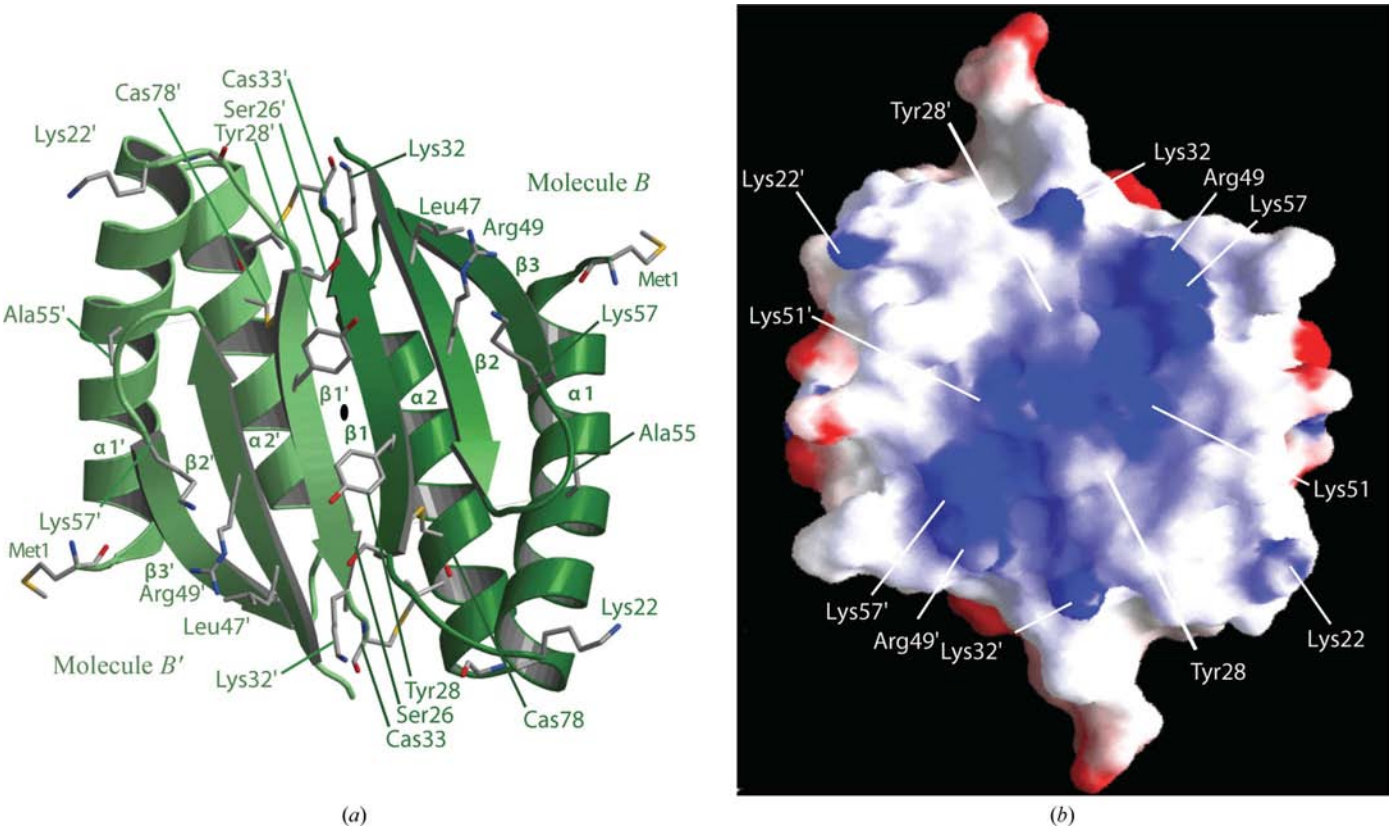

Figure 3
A homodimeric SRP14. (*a*) One molecule of *S. pombe* SRP14 (chain *B*) and its binding partner related by crystallographic symmetry, the axis of which is indicated by the graphical symbol for a twofold rotation axis normal to the plane of the figure. (*b*) Electrostatic potential surface of the SRP14 homodimer shown in (*a*) displayed using *GRASP* (Nicholls *et al.*, 1991). In both cases, amino acids which are likely to be of functional importance are labelled.

The As *K* edge is at a lower energy than that of selenium (11.867 keV, 1.04 Å for As *versus* 12.658 keV, 0.98 Å for Se). Theoretically, the real and imaginary components of the arsenic scattering factor at 0.98 Å are of sufficient magnitude (f' of ~-1.8 electrons and f'' of ~3.4 electrons) to detect anomalous signal from ordered As atoms even at the selenium edge. Therefore, this was a potentially useful, albeit sub-optimal, wavelength for the location of any arsenic heavy-

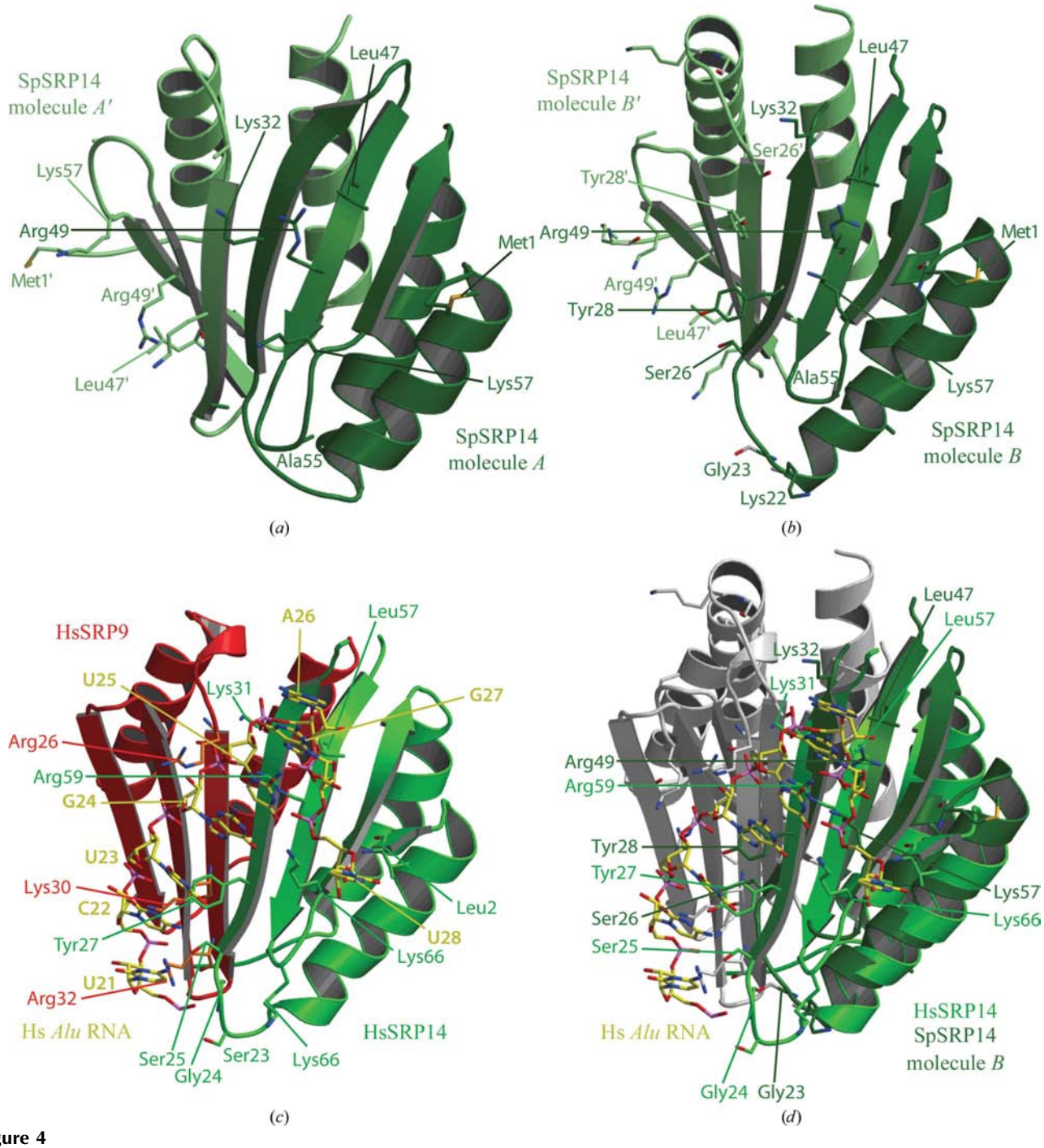

Figure 4
Structural conservation of residues of SpSRP14 which are likely to interact with RNA. (*a*) The homodimer of SpSRP14 *A* molecules and (*b*) the homodimer of SpSRP14 *B* molecules, with structurally conserved residues shown as sticks (see text and Table 4 for further details). SpSRP14 *A* and *B* molecules are shown in dark green and crystallographically related molecules (*A*′ and *B*′) are coloured light green. The sticks are blue for nitrogen, red for oxygen and yellow for sulfur. (*c*) The *H. sapiens* SRP9/14 heterodimer is depicted with nucleotides 20–28 of *Alu* RNA (Weichenrieder *et al.*, 2000), the sequence predicted to be similar in structure to the fungal U-turn motif (Wild *et al.*, 2002). Colouring is as according to (*a*) and (*b*), except that SRP9 and SRP14 are shown as red and green cartoons, respectively. RNA C atoms are coloured yellow, SRP9 C atoms are orange and SRP14 C atoms are green. Residues which interact with the RNA are shown in stick representation, as is the RNA. (*d*) *S. pombe* SRP14 molecule *B* was superposed with the human SRP14 using *SSM* (Krissinel & Henrick, 2003). Only the residues which are strictly conserved between *S. pombe* and human SRP14 subunits are labelled and only the superposed SRP14 molecules and the RNA are coloured in the interests of clarity.

Table 4
Sequence conservation of SRP14 subunits.

H. sapiens	*S. pombe*	Identical/ conserved	Ligand ribonucleotide
Leu2	Met1	−/+	PO_4 C29
Ser23	Lys22	−/−	PO_4 C21
Gly24	Gly23	+/+	PO_4 C22
Ser25	Ser26	+/+	PO_4 C22
Tyr27	Tyr28	+/+	PO_4 U23
Lys31	Lys32	+/+	PO_4 U25, PO_4 A26
Leu57	Leu47	+/+	PO_4 A26
Arg59	Arg49	+/+	PO_4 U25
Lys64	Ala55	−/−	PO_4 C19
Lys66	Lys57	+/+	PO_4 U28, PO4 G24

atom substructure by virtue of the anomalous scattering of such atoms at this energy.

The X-ray crystal structure of fission yeast SRP14 revealed that the two molecules in the asymmetric unit are surprisingly dissimilar, with maximal r.m.s. deviations of C^{α} atoms of 6.7 Å in strand β1 (Fig. 2*b*). While both dimer interfaces form continuous canonical β-sheets, the register of strand β1 has been shifted in chain *A* by two residues. This distortion may arise from the steric effects imposed by the cacodylated cysteine residues, but the displacement of this sequence also indicates flexibility of the β-strands within this zone. Since the two molecules differ so dramatically, the dimer interfaces also differ significantly: 1317 Å^2 for the dimer of *B* molecules and 1055 Å^2 for the dimer of *A* molecules, as calculated by *PISA* (Krissinel & Henrick, 2007).

Superimposition of the two NCS-related molecules demonstrates the significant differences in position and orientation between the Cas residues in each chain and these participate in the formation of crystal contacts (Fig. 2*a*). Cas33 of chain *A* contacts Lys32*A*, Asn34*A*, Val46*A*, Ile48*A* and Phe71*A* from the same molecule, as well as Leu29*A*, Gln31*A*, Tyr74*A* and Cas78*A* of a symmetry mate. In contrast, the equivalent residue of chain *B* contacts only three residues: Lys32*B*, Asn34*B* and Val46*B* of the same chain. The arsenic of Cas78*A* interacts with Tyr74*A*, Val77*A* and Ala79*A* of its own chain, as well as forming crystal contacts with Cas33*A* and Phe67*A* of a symmetry-related molecule. A denser network of interactions is found around Cas78*B*; it contacts Val77*B*, Lys79*B*, Gln81*B* and Ile82*B* of the same chain as well as Gln31*B* and Phe67*B* of symmetry-related molecules.

In this structure, cacodylated cysteine residues form intersubunit interactions which fasten the SpSRP14 dimers together *via* residues Cas33 and Cas78. The distance between the As atoms of Cas33*A* and Cas78*A*′ is 4.7 Å and that between those of Cas33*B* and Cas78*B*′ is 5.3 Å. van der Waals forces around both As atoms are essential to the formation of crystal contacts and we did not find it possible to obtain crystals without the use of cacodylate buffer in the mother liquor. It is notable that Cys39 of murine SRP9 has also been shown to be reactive; during the purification procedure prior to crystallization of the murine SRP9/14 fusion protein this residue had reacted with β-mercaptoethanol (Birse *et al.*, 1997). The reactivity of the *Alu*-domain cysteine residues may well be physiologically important, although it is not yet clear in what way. Certain cysteine residues are conserved amongst SRP9 and SRP14 homologues, projecting out from the β-sheet towards the RNA-binding face in the murine structure (Birse *et al.*, 1997). However, the cysteine residues in the *S. pombe* structure and those in the murine structure are not conserved; only one of the two residues is located in the β-sheet, but it faces towards the interior of the protein (Figs. 1 and 2).

4. Discussion

4.1. The probable biological dimer of *S. pombe* SRP14

There are two molecules of SpSRP14 in the asymmetric unit which are in appreciably different conformations, but it was not immediately apparent which of them corresponds to the physiologically relevant form. In order to determine which conformation is most likely to represent SpSRP14 *in vivo*, it was informative to compare each chain with the previous structure of *Homo sapiens* SRP14 (Weichenrieder *et al.*, 2000). Two main observations indicate that chain *B* is more representative of the natural form (Figs. 2 and 4). Firstly, chain *A* is the more disordered of the two molecules and one of the conserved residues which is predicted to interact with RNA and is situated on β-strand 1, Tyr28*A*, is not clearly visible in electron density. This residue is truncated at the C^{β} atom in the atomic model. While Tyr28*B* is positioned relatively similarly to the conserved human residue, Tyr27 (Fig. 4), the stub of Tyr28*A* is excessively displaced relative to it. We believe this conformation to be less likely to bind efficiently to RNA given the role of human Tyr27 in contacting U23. Secondly, the buried surface area (BSA) of the dimer interface of the chain *A* molecules is significantly smaller than that of the dimer of chain *B* molecules, as stated above. Indeed, the human SRP9/14 complex buries a surface area of 1500 Å^2 (Weichenrieder *et al.*, 2000), which is roughly similar to the dimer of SpSRP14 *B* molecules (1317 Å^2). Owing to these considerations, the dimer of chain *B* molecules is taken to be the most probable multimeric state (Fig. 3).

4.2. Structural conservation of residues on the RNA-binding face of SpSRP14

The human SRP9/14 complex binds to a conserved U-turn sequence at the core of a pseudoknot structure of 7SL RNA (human SRP RNA), represented in that structure by the SA50 RNA construct. It also has a second lower affinity binding site which is located on helix 5 of 7SL RNA (Weichenrieder *et al.*, 2000, 2001; Fig. 1*b*). SA50 RNA is tilted towards SRP14 and relatively few contacts are made with SRP9; these are clustered along the first β-strand and involve residues Arg26, Lys30 and Arg32. Residues on the β-sheet face of SRP14 make the remaining contacts with the SA50 RNA.

A hairpin loop at the 5′-end of s1r1 RNA has been proposed to be the binding site of the *S. pombe* proteins, which has been supported by the results of random mutagenesis (Liao *et al.*, 1992). Despite the modest size of this hairpin compared with the human pseudoknot, the sequence probably

Table 5
Map correlation coefficients.

Source of phase information	RIP	Combined	DM	$2F_o - F_c$
SAD	0.156	0.803	0.522	0.526
RIP		0.655	0.424	0.444
Combined			0.646	0.661
DM				0.814

also contains a U-turn motif which should be sufficient to be recognized by the *Alu*-domain proteins (Wild *et al.*, 2002). More importantly, chemical footprinting of *S. cerevisiae Alu* RNA using SRP14p showed that this U-turn motif was one of the two sites which were the most protected. The RNA-binding face of the SpSRP14 homodimer could therefore be capable of binding its cognate RNA in a similar manner to that found in the human and yeast complexes. However, it is not yet clear whether there is a second site of protein contacts on fission yeast RNA.

In order to predict the residues which were involved in s1r1 recognition, we have analyzed the structural conservation of residues on the potential RNA-binding face of SpSRP14. The human and *S. pombe* SRP14 sequences have approximately 34% sequence identity (36 identical of 106 aligned residues) and a significant number of residues are highly conserved (Fig. 1; asterisks indicate human residues which contact RNA in the SRP9/14–SA50 complex; Weichenrieder *et al.*, 2000). Residues which are positioned similarly to those of human SRP14 are depicted in Fig. 3(*a*) and the conservation of such residues is tabulated in Table 4. Additionally, the charged nature of the RNA-binding face of SpSRP14 is evident when an electrostatic potential is mapped onto the surface of the homodimer (Fig. 3*b*; conserved RNA-binding residues are labelled); the lysine and arginine side chains contribute to the formation of a basic surface which is well disposed for interaction with the phosphate backbone of RNA.

Arg49 is strictly conserved amongst the sequences presented in Fig. 1. Indeed, this residue is conserved amongst virtually all SRP14 subunits known at present (Rosenblad *et al.*, 2003). The corresponding residue in the human complex, Arg59, bridges the phosphates of the U-turn motif and we believe it is probable that the *S. pombe* residue will fulfil a generally similar role in its interaction with s1r1 RNA. Mutation of the orthologous residue in *S. cerevisiae*, Arg81, to alanine abrogated the RNA-binding activity of SRP14p, underscoring its importance even in the yeast complexes (Strub *et al.*, 1999).

S. pombe Tyr28 and Lys57 are conserved in human SRP14 as Tyr27 and Lys66, respectively. In the crystal structure of human Srp9/14 with SA50 RNA, Tyr27 contacts the phosphate U23, while Lys66 participates in a base-specific interaction with G24 of the UGUNR (U-turn) sequence which is conserved in yeasts (Fig. 4; Weichenrieder *et al.*, 2000). Lys31 of human SRP14 (Lys32 in *S. pombe*, also strictly conserved in Fig. 1) contacts U25 and A26 of SA50 RNA and this residue is similarly placed in the fission yeast structure. The double mutation K35A/R36A of *S. cerevisiae* SRP14p (Lys32 and Cys32 in fission yeast) abolished its capacity to bind RNA (Strub *et al.*, 1999), suggesting that one or both of these residues participate in contacts with RNA. In short, various structurally conserved SpSRP14 residues are likely to contribute to the recognition of s1r1 *Alu* RNA in a manner which is generally analogous to that observed in the human *Alu*-domain complex.

On the α-helical face of SpSRP14, there is little conservation of either charge or sequence. However, a small acidic region is present on α-helix 2, comprising the negatively charged residues Glu63, Asp65, Asp69 and Glu76, with additional acidic residues being found on helix 1, notably Glu6, which is highly conserved, and Glu7. A similar charged site on α-helix 1 of SRP14 has previously been observed on the electrostatic potential surface of the mouse homologue (Birse *et al.*, 1997).

4.3. Utility of the phasing strategy

Single-wavelength anomalous dispersion (SAD) experiments are frequently employed when multiple-wavelength (MAD) experiments fail. However, the phases resulting from such SAD experiments have bimodal probability distributions, the ambiguity of which is usually resolved by density modification (Cowtan, 1994; Terwilliger, 2003*b*). The solvent content of these crystals, taking into account both chains of 91 residues, is 40%, so density modification would not be expected to give rise to much of an improvement in the phases in this case. This particular structure determination was designed from the outset to couple SAD phases with those of RIP in order to obtain a unimodal joint phase probability distribution and to

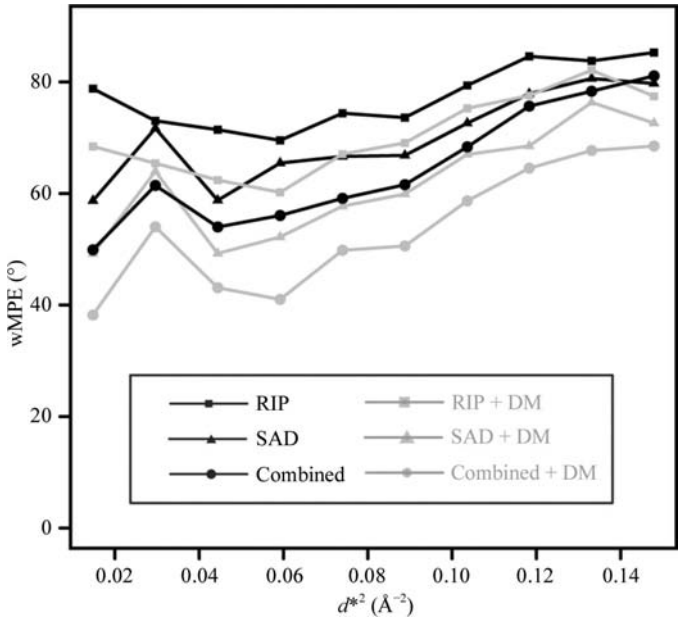

Figure 5
Mean weighted phase errors (wMPE) compared with the phases of the refined structure are plotted *versus* resolution at various stages of the structure determination. SAD phases are indicated by squares, RIP phases by triangles and combined phases by circles. The curves corresponding to experimental phases are coloured black and those for each phase set after density modification are coloured grey.

derive more accurate phases than SAD alone could provide (Evans *et al.*, 2003; Banumathi *et al.*, 2004; Nanao *et al.*, 2005). Presentations of the basis for this type of experiment as well as potential pitfalls have been described elsewhere (Zwart *et al.*, 2004; Ravelli *et al.*, 2005; Ramagopal *et al.*, 2005).

Once the structure had been solved, the question arose of how much of an improvement was gained by incorporating RIP phases instead of SAD phases alone. To answer, electron-density maps were calculated from each of the following: (i) SAD phases alone, (ii) RIP phases alone, (iii) combined phases from both (i) and (ii) above, (iv) density modification of the combined phases and (v) a $2F_o - F_c$ map from the final refined model. Correlation coefficients (CCs) between each of these maps were then calculated using *MAPMAN* (Kleywegt & Jones, 1996) and a matrix of the resulting CCs is shown in Table 5. Additionally, the weighted mean phase errors (wMPEs) of each phase set compared with calculated structure factors for the final model were calculated using *PHISTATS* (Collaborative Computational Project, Number 4, 1994) and these were plotted as a function of resolution (Fig. 5).

Comparison of the wMPEs demonstrates that the phases obtained from RIP were much less accurate than those of SAD from the combined data set (76.8° and 67.0° overall, respectively, from 40 to 2.6 Å resolution). A similar conclusion may be drawn from the map CCs between the SAD and the $2F_o - F_c$ maps (0.526) and between the RIP and the $2F_o - F_c$ maps (0.444; Figs. 6*a*, 6*b* and 6*d*). However, it is notable that the electron-density map from RIP does appear to be interpretable in parts, notably around the heavy-atom sites (Fig. 6*d*), and RIP alone was therefore capable of solving the structure. This conclusion is reiterated by the wMPE of RIP (Fig. 5), which is 76.8° and therefore better than random. The utility of including phases obtained by modelling specific sites which are susceptible to radiation damage is also indicated by the isomorphous phasing power (0.995 for acentric, 0.782 for centric reflections; Table 2). These poor RIP phases were nonetheless useful in this case, firstly to improve on the SAD phases for map calculation and secondly to help in refinement of the atomic model, which was challenging even when the Hendrickson–Lattman coefficients of these combined phases were incorporated into the maximum-likelihood target function (Pannu *et al.*, 1998).

Both the SAD and RIP maps suffered from very poor connectivity, which would make model building problematic. Density modification of either the RIP or the SAD phases

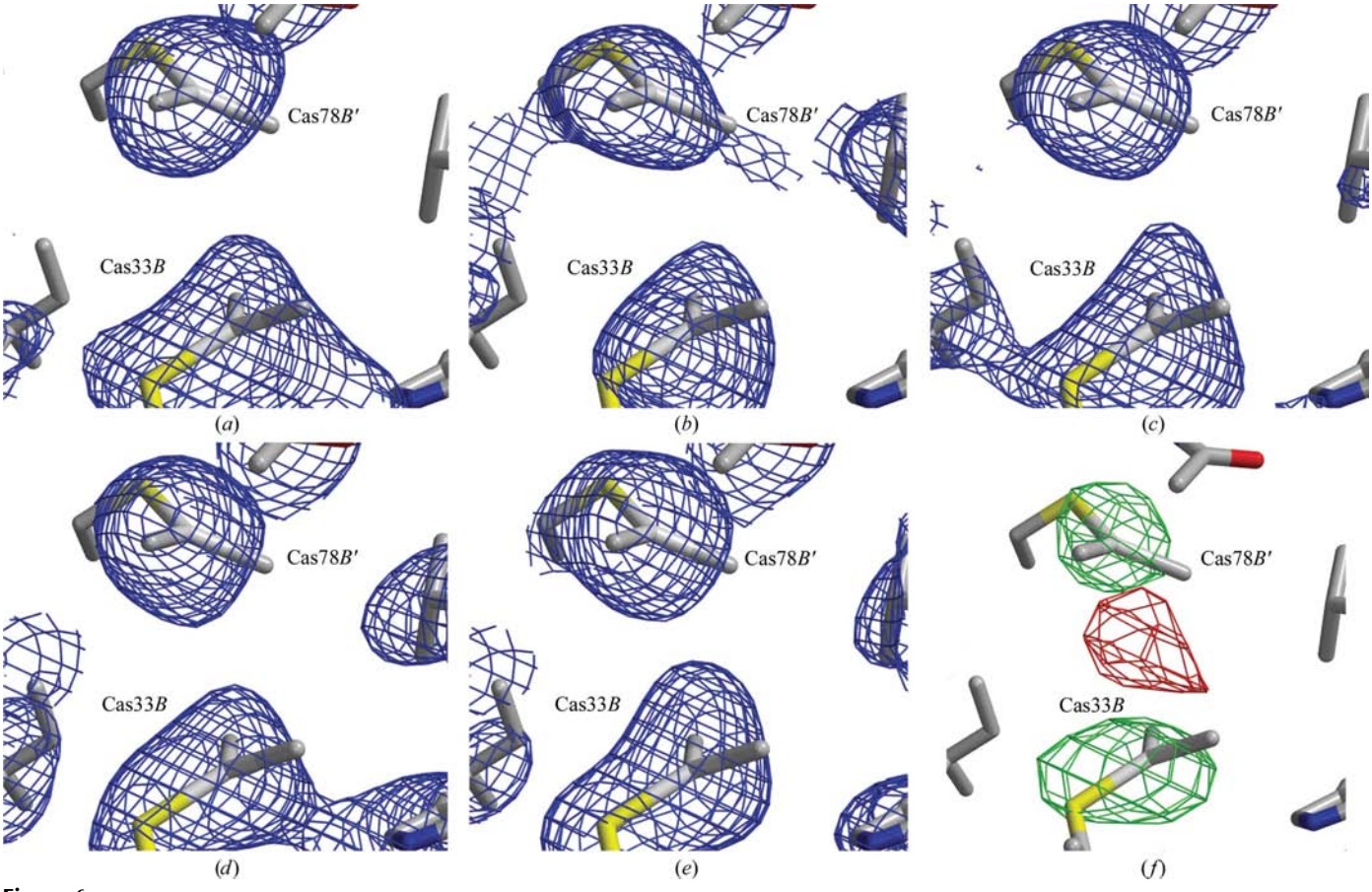

Figure 6
Electron density is shown around Cas78*B* of one molecule and Cas33*B* of a molecule related by crystallographic symmetry, corresponding to (*a*) SAD phases, (*b*) RIP phases, (*c*) combined phases from SAD and RIP, (*d*) density modification of (*c*), (*e*) $2F_o - F_c$ map from *REFMAC* and (*f*) $F_o - F_o$ difference density map. This figure was produced using *BOBSCRIPT* (Esnouf, 1997). Atoms are shown as sticks coloured as follows: carbon, grey; sulfur, yellow; nitrogen, blue; oxygen, red; arsenic, white. The electron density is contoured at 1.5σ, except for in (*f*), where positive density was contoured at 4σ and negative density at -4σ.

yielded electron density which was only partially interpretable and the imperfection of the noncrystallographic symmetry (NCS) limited its usefulness for the purpose of NCS averaging (data not shown). Nevertheless, density modification of each of these phase sets produced a reduction in phase errors compared with the calculated phases of the final model (Fig. 6). Combination of the experimental SAD and RIP phase sets with *SIGMAA* (Read, 1986) resulted in a markedly improved electron density (Fig. 6*c*), which was largely continuous along the polypeptide chains even prior to density modification. This is reflected in a higher map CC between the phase-combined and the final refined map (0.661) and an overall wMPE of 62.6°. There was again a further enhancement in the phase accuracy yielded by density modification and this is reflected in the improvement of the CC between the map calculated using density-modified combined phases and the $2F_o - F_c$ map to 0.814 and a wMPE of 51.6°. This map was used to construct the atomic model and *RESOLVE* (Terwilliger, 2003*a*) successfully traced the majority of the protein backbone of SpSRP14 starting from these density-modified phases.

The location of the sites of the radiation damage, demonstrated by an $F_o - F_o$ map (data set 1 − data set 3), are centred mainly upon the heavy atoms (Fig. 6), with both positive and negative density around the As atoms of Cas78*B* and Cas33*B*. It has been noted previously that S–Hg adducts are susceptible to radiation damage, which can lead to problems when phasing using traditional MAD or SAD protocols (Ramagopal *et al.*, 2005). This case exemplifies a similar phenomenon with respect to S–As adducts and is the first time to our knowledge that X-ray radiation-mediated breakage of such bonds has been observed.

Additional sites of damage include Glu7*B* and Asp14*B*, which appear to be decarboxylated upon exposure to X-rays. Such damage to acidic side chains as well as to carboxy-termini is observed frequently upon the exposure of macromolecular crystals to synchrotron radiation (Burmeister, 2000; Ravelli & McSweeney, 2000). The carboxy-termini of both chains of this structure are disordered and therefore we do not know whether these moieties are intact. Somewhat surprisingly, there were no major peaks in the $F_o - F_o$ map around the Se atoms, perhaps as a consequence of the mobility of these amino-terminal residues.

In the SAD component of the experiment, two Se atoms corresponding to two rotamers of the initiating methionine of chain *A* were located by *SHELXD*. Additionally, three of the four bound As atoms were correctly identified by this program. Therefore, by performing SAD at the Se *K* edge, the sites of both Se and As atoms may be located. This may be useful for other structure-solution experiments in which arsenic is incorporated into the crystals, whether from the mother liquor (Greenwald *et al.*, 1999) or from the addition of extraneous arsenic-containing compounds (Retailleau & Prangé, 2003).

The reaction of cacodylate with cysteine side chains has now provided useful heavy-atom sites for *de novo* structure solution in (at least) two cases, that considered here as well as that of HIV integrase (Greenwald *et al.*, 1999), and may well find further applications. For proteins such as SpSRP14, the reaction of cacodylate with sulfhydryl groups under reducing conditions may allow novel crystal contacts to be obtained. The methylation of lysine residues as a strategy to obtain crystals of recalcitrant proteins has been documented (Walter *et al.*, 2006) and we believe that in the future it is likely that the formation of cacodylate adducts will serve to induce crystallization of other proteins of interest in an analogous manner.

5. Summary

The phasing strategy used here had been proposed previously as a way of extracting more accurate phase information than SAD alone can provide (Ravelli *et al.*, 2003, 2005; Zwart *et al.*, 2004; Banumathi *et al.*, 2004; Evans *et al.*, 2003). Indeed, the electron-density maps of SRP14 were greatly improved by this method, largely owing to the radiation-sensitivity of the S—As bond. RIP appears to be particularly useful when MAD has failed, since these isomorphous differences provide an indicator that the heavy atoms of the sample being irradiated may be vulnerable to X-rays (Ramagopal *et al.*, 2005). By taking advantage of the phases garnered from RIP(AS), the deleterious effects that electromagnetic radiation has on biological samples which contain bound arsenic may be offset, at least in part, by the helpful improvement in electron-density maps that radiation damage provides.

In summary, the crystal structure presented here shows that SpSRP14 forms homodimers, although it is possible that this oligomeric state is favoured under the crystallization conditions by cacodylated cysteine residues, which form intersubunit contacts. However, the fact that the crystallized SpSRP14 protein was co-expressed and copurified with SpSRP21 suggests that no stable heterodimer exists between these two components, providing additional indirect evidence for a functional SpSRP14 homodimer. The existence of such a homodimer has already been established for the *Saccharomyces cerevisiae* homologue (SRP14p; Strub *et al.*, 1999; Mason *et al.*, 2000), although since the SRP RNAs of *Saccharomyces cerevisiae* and *Schizosaccharomyces pombe* are very different caution needs to be maintained with respect to any analogy between the two yeasts. From the known structure of the human *Alu*-domain proteins in complex with *Alu* RNA it is possible to draw various conclusions about which SpSRP14 residues are likely to contact the RNA and the probable similarity of the nucleic acid recognition between yeast-type SRPs and those of higher eukaryotes.

Upon publication of the structure of the murine SRP9/14 complex, in which it was elucidated for the first time that the two molecules form a pseudo-symmetrical heterodimer, the authors proposed a theory in which an ancestral complex had initially been a homodimer which evolved into a heterodimer by gene duplication 'to accommodate asymmetry' (Birse *et al.*, 1997). Because they were aware that no SRP9 homologue had been identified in the yeast genome at that time, they speculated that *S. cerevisiae* either possesses an SRP14 monomer or a homodimer. The structure presented here of the fission yeast homologue lends strong weight to the latter of their hypo-

theses. However, it still remains a puzzle how a presumed symmetric homodimer could interact with a single asymmetric RNA structure, although our observation of structural flexibility in the register of one of the β-strands may be relevant in this context.

The authors wish to acknowledge the European Union Framework IV TMR for SRPNET (FMRX-CT960035) and Framework V Quality of Life programme for MEMPROTNET (QLK3-CT200082) for funding MAB. The beamline staff of the EMBL and ESRF and in particular Gordon Leonard and Didier Nurizzo (both from the ESRF) and Max Nanao (formerly of EMBL) are thanked for expert advice.

References

Banumathi, S., Zwart, P. H., Ramagopal, U. A., Dauter, M. & Dauter, Z. (2004). *Acta Cryst.* D**60**, 1085–1093.

Barton, G. J. (1993). *Protein Eng.* **6**, 37–40.

Birse, D. E., Kapp, U., Strub, K., Cusack, S. & Aberg, A. (1997). *EMBO J.* **16**, 3757–3766.

Blobel, G. & Dobberstein, B. (1975*a*). *J. Cell Biol.* **67**, 835–851.

Blobel, G. & Dobberstein, B. (1975*b*). *J. Cell Biol.* **67**, 852–862.

Boomershine, W. P., Raj, M. L. S., Gopalan, V. & Foster, M. P. (2003). *Protein Expr. Purif.* **28**, 246–251.

Brown, J. D., Hann, B. C., Medzihradszky, K. F., Niwa, M., Burlingame, A. L. & Walter, P. (1994). *EMBO J.* **13**, 4390–4400.

Burmeister, W. P. (2000). *Acta Cryst.* D**56**, 328–341.

Collaborative Computational Project, Number 4 (1994). *Acta Cryst.* D**50**, 760–763.

Connolly, T., Rapiejko, P. J. & Gilmore, R. (1991). *Science*, **252**, 1171–1173.

Cowtan, K. (1994). *Jnt CCP4/ESF–EACBM Newsl. Protein Crystallogr.* **31**, 34–38.

Davis, I. W., Murray, L. W., Richardson, J. S. & Richardson, D. C. (2004). *Nucleic Acids Res.* **32**, W615–W619.

Emsley, P. & Cowtan, K. (2004). *Acta Cryst.* D**60**, 2126–2132.

Esnouf, R. M. (1997). *J. Mol. Graph. Model.* **15**, 132–134.

Evans, G., Polentarutti, M., Djinovic Carugo, K. & Bricogne, G. (2003). *Acta Cryst.* D**59**, 1429–1434.

Gilmore, R., Blobel, G. & Walter, P. (1982). *J. Cell Biol.* **95**, 463–469.

Greenwald, J., Le, V., Butler, S. L., Bushman, F. D. & Choe, S. (1999). *Biochemistry*, **38**, 8892–8898.

Halic, M., Becker, T., Pool, M. R., Spahn, C. M. T., Grassucci, R. A., Frank, J. & Beckmann, R. (2004). *Nature (London)*, **427**, 808–814.

Jones, T. A., Zou, J.-Y., Cowan, S. W. & Kjeldgaard, M. (1991). *Acta Cryst.* A**47**, 110–119.

Kabsch, W. (1993). *J. Appl. Cryst.* **26**, 795–800.

Keenan, R. J., Freymann, D. M., Stroud, R. M. & Walter, P. (2001). *Annu. Rev. Biochem.* **70**, 755–775.

Kendrew, J. C., Bodo, G., Dintzis, H. M., Parrish, R. G., Wyckoff, H. & Phillips, D. C. (1958). *Nature (London)*, **181**, 662–666.

Kleywegt, G. J. & Jones, T. A. (1996). *Acta Cryst.* D**52**, 826–828.

Kraulis, P. J. (1991). *J. Appl. Cryst.* **24**, 946–950.

Krissinel, E. & Henrick, K. (2003). *Proceedings of the 5th International Conference on Molecular Structural Biology*, edited by J. Kungl & P. J. Kungl, p. 88. Vienna: Austrian Chemical Society.

Krissinel, E. & Henrick, K. (2007). *J. Mol. Biol.* **372**, 774–797.

La Fortelle, E. de & Bricogne, G. (1997). *Methods Enzymol.* **276**, 472–494.

Lakkaraju, A. K. K., Mary, C., Scherrer, A., Johnson, A. E. & Strub, K. (2008). *Cell*, **133**, 440–451.

Liao, X., Selinger, D., Althoff, S., Chiang, A., Hamilton, D., Ma, M. & Wise, J. A. (1992). *Nucleic Acids Res.* **20**, 1607–1615.

Maignan, S., Guilloteau, J. P., Liu, Q. Z., Mella, C. C. & Mikol, V. (1998). *J. Mol. Biol.* **282**, 359–368.

Maniatis, T., Fritsch, E. F. & Sambrook, J. (1982). *Molecular Cloning, A Laboratory Manual.* Cold Spring Harbor, New York: Cold Spring Harbor Laboratory.

Mason, N., Ciufo, L. F. & Brown, J. D. (2000). *EMBO J.* **19**, 4164–4174.

Moreno, S., Klar, A. & Nurse, P. (1991). *Methods Enzymol.* **194**, 795–823.

Murshudov, G. N., Vagin, A. A. & Dodson, E. J. (1997). *Acta Cryst.* D**53**, 240–255.

Nanao, M. H., Sheldrick, G. M. & Ravelli, R. B. G. (2005). *Acta Cryst.* D**61**, 1227–1237.

Nicholls, A., Sharp, K. A. & Honig, B. (1991). *Proteins*, **11**, 281–296.

Ogg, S. C. & Walter, P. (1995). *Cell*, **81**, 1075–1084.

Pannu, N. S., Murshudov, G. N., Dodson, E. J. & Read, R. J. (1998). *Acta Cryst.* D**54**, 1285–1294.

Ramagopal, U. A., Dauter, Z., Thirumuruhan, R., Fedorov, E. & Almo, S. C. (2005). *Acta Cryst.* D**61**, 1289–1298.

Ravelli, R. B. G., Leiros, H.-K. S., Pan, B., Caffrey, M. & McSweeney, S. (2003). *Structure*, **11**, 217–224.

Ravelli, R. B. & McSweeney, S. M. (2000). *Structure Fold. Des.* **8**, 315–328.

Ravelli, R. B. G., Nanao, M. H., Lovering, A., White, S. & McSweeney, S. (2005). *J. Synchrotron Rad.* **12**, 276–284.

Read, R. J. (1986). *Acta Cryst.* A**42**, 140–149.

Retailleau, P. & Prangé, T. (2003). *Acta Cryst.* D**59**, 887–896.

Rigaut, G., Shevchenko, A., Rutz, B., Wilm, M., Mann, M. & Séraphin, B. (1999). *Nature Biotechnol.* **17**, 1030–1032.

Rosenblad, M. A., Gorodkin, J., Knudsen, B., Zwieb, C. & Samuelsson, T. (2003). *Nucleic Acids Res.* **31**, 363–364.

Rosenblad, M. A., Zwieb, C. & Samuelsson, T. (2004). *BMC Genomics*, **5**, 5.

Selinger, D., Brennwald, P., Althoff, S., Reich, C., Hann, B., Walter, P. & Wise, J. A. (1994). *Nucleic Acids Res.* **22**, 2557–2567.

Sheldrick, G. M. (2008). *Acta Cryst.* A**64**, 112–122.

Strub, K., Fornallaz, M. & Bui, N. (1999). *RNA*, **5**, 1333–1347.

Strub, K. & Walter, P. (1990). *Mol. Cell. Biol.* **10**, 777–784.

Tan, S. (2001). *Protein Expr. Purif.* **21**, 224–234.

Terwilliger, T. C. (2003*a*). *Acta Cryst.* D**59**, 38–44.

Terwilliger, T. C. (2003*b*). *Acta Cryst.* D**59**, 1688–1701.

Terzi, L., Pool, M. R., Dobberstein, B. & Strub, K. (2004). *Biochemistry*, **43**, 107–117.

Thomas, Y., Bui, N. & Strub, K. (1997). *Nucleic Acids Res.* **25**, 1920–1929.

Thompson, J. D., Gibson, T. J., Plewniak, F., Jeanmougin, F. & Higgins, D. G. (1997). *Nucleic Acids Res.* **25**, 4876–4882.

Walter, P. & Blobel, G. (1981). *J. Cell Biol.* **91**, 557–561.

Walter, T. S., Meier, C., Assenberg, R., Au, K.-F., Ren, J., Verma, A., Nettleship, J. E., Owens, R. J., Stuart, D. I. & Grimes, J. M. (2006). *Structure*, **14**, 1617–1622.

Weichenrieder, O., Stehlin, C., Kapp, U., Birse, D. E., Timmins, P. A., Strub, K. & Cusack, S. (2001). *RNA*, **7**, 731–740.

Weichenrieder, O., Wild, K., Strub, K. & Cusack, S. (2000). *Nature (London)*, **408**, 167–173.

Wild, K., Weichenrieder, O., Strub, K., Sinning, I. & Cusack, S. (2002). *Curr. Opin. Struct. Biol.* **12**, 72–81.

Zvelebil, M. J., Barton, G. J., Taylor, W. R. & Sternberg, M. J. (1987). *J. Mol. Biol.* **195**, 957–961.

Zwart, P. H., Banumathi, S., Dauter, M. & Dauter, Z. (2004). *Acta Cryst.* D**60**, 1958–1963.